Laser Induced Fluorescence Characterization of Ions Emitted from Hollow Cathodes

George J. Williams, Jr.[*], Timothy B. Smith[*], Matthew T. Domonkos[*], Karyl J. Shand[**], Alec D. Gallimore[=] and R. Paul Drake[==]

Laser induced fluorescence (LIF) was used to measure the mean and variance of the velocity distribution of xenon ions emitted from two hollow cathode assemblies operating at low power. High-energy ions detected in plume-mode and spot-mode operation are consistent with the potential-hill model of high-energy ion production. The distributions of velocities were modeled, yielding temperatures on the order of a few eV in plume-mode and one eV in spot-mode. LIF of neutral xenon atoms in the plumes indicated thermal temperatures significantly less than the temperatures associated with the ion velocity distributions.

Nomenclature

c	Speed of light, $2.998 \cdot 10^{8}$ m/s
g()	Normalized Gaussian lineshape
e	Electron charge, $1.6022 \cdot 10^{-19}$ C
E	Electric field strength (V/m)
F	Total axial force applied to the gas (N)
J_{si}	Ion saturation current flux (A/cm^2)
k	Boltzmann constant, $1.3807 \cdot 10^{-23}$ J/K
m_e	Mass of an electron (kg)
m_i	Mass of an ion (kg)
m	heavy particle mass (kg)
n	Number density (cm^{-3})
r	radial position (m)
t	time (s)
T_e	Electron Temperature (K)
v	Speed (m/s)
z	Distance from cathode
λ	Wavelength (nm)
μ	Permeability of free space, $4\pi \cdot 10^{-7}$ H/m
ν	Frequency (1/s)
ρ	Heavy particle mass density (kg/m^3)
σ	Heavy particle collision cross-section (m^2)
Ω	Solid angle
ln(A)	Coulomb logarithm

Introduction

Electric propulsion devices such as ion engines and Hall thrusters are emerging as replacements for chemical rockets on satellites and planetary probes because they use significantly less propellant as a result of their higher specific impulse. Long life, orificed hollow cathodes are generally considered to be required as the electron sources for these propulsion systems.[1]

Severe erosion of electrodes and structures, such as the cathode heater, near hollow cathodes operating at high emission currents (a few tens of amperes) could limit the lifetime of these engines.[2] A 2000 hr test conducted at the NASA Glenn Research Center (GRC) identified discharge cathode assembly erosion as one of the primary potential failure mechanisms resulting from long-term operation.[3] Employment of a keeper electrode has provided an engineering solution for the current NSTAR configuration.[4] However, a greater understanding of the physical phenomena associated with cathode operation is required for confidence in further thruster development.

The cause of this erosion is believed to be high-energy ions produced near the hollow cathode orifice. Friedly and Wilber proposed that the high energy of the ions (significantly higher than the cathode to anode fall voltage) may result from

[*] Graduate Student, Student Member, AIAA.
[**] Undergraduate Student, Student Member, AIAA.
[=] Associate Professor and Director of Lab, Associate Fellow, AIAA.
[==] Professor.

production of these ions near the maximum of a potential profile near the cathode. The ions would be accelerated to high kinetic energies as they moved off the potential-hill.[5] Data obtained by electrostatic energy analyzer (ESA) and by retarding potential analyzer (RPA) confirm the existence of the high-energy ions and indicate that these ions are emitted in a roughly collimated beam away from the cathode.[1,2]

To avoid perturbing cathode operation and/or melting of the probe, Langmuir probe measurements are typically not made within about 0.5 cm of the cathode orifice.[5] Because it is non-intrusive, laser induced fluorescence (LIF) has been used under similar conditions to measure plasma properties.[6,7,8] LIF is particularly attractive in this case because of the small physical dimensions and the locally high plasma density ($>10^{14}$ cm^{-3})[5]. Verification of the "potential hill" model or discovery of another means of high-energy ion production will provide the confidence necessary for development of many electric propulsion devices, especially ion engines.

Theory

Laser Induced Fluorescence

Laser induced fluorescence (LIF) is the incoherent emission of photons from an unstable energy level (electronic in the case of xenon or other monatomics) populated by the absorption of photons from the laser. In general, the energies (wavelengths) of the absorbed and emitted photons are different. Indeed, emission may occur at many different wavelengths.

The absorbing neutral xenon, Xe I, or singly ionized xenon, Xe II, will "see" the wavelength of the incoming photons shifted by the relative motion of the ion in the direction of the photon. This Doppler effect is seen as spectral line broadening due to the random thermal (Maxwellian) or artificial (accelerated) variations in absorber motion. It is seen as a potentially large Doppler shift due to a bulk velocity. In either case, the change in photon frequency ν is

$$\Delta\nu = \nu_0 \cdot \left({}^{v_i}\!/\!_{c} \right). \qquad (1)$$

Xe I and Xe II have natural absorption/ emission transitions throughout the visible spectrum. Xe II LIF was stimulated at the $5d^4D$—$6p^4P^0$ (605.28 nm) transition, and emission at the $6s^4P$—$6p^4P^0$ (529 nm) transition was selected for collection, as it has the strongest emission available from the $6s^4P^0$ state. Xe I LIF was stimulated at the $6s'[1/2]^0$—5f[11/2] (582.5 nm) transition, and emission at the $6s'[1/2]^0$—5f[11/2] (617.97 and 617.83 nm) transitions was collected.

A dual-beam configuration interrogated the plasma. This permitted simultaneous measurements of radial and axial velocity components.[9] The beams were split just downstream of the dye laser as shown in Fig. 1. The beam passing perpendicular to the axis of the cathode directly measured the radial component of velocity and is referred to below as the "radial" beam. The other beam measured the velocity in the direction of the beam which has both radial and axial components. Because it was used to determine the axial component, it is referred to below as the "axial" beam. The axial velocity component, v_A, can be deduced from the radial velocity, v_R, and the off axis velocity, v_O,

$$v_A = \frac{v_O - v_R \cos(\alpha)}{\sin(\alpha)}, \qquad (2)$$

as illustrated in Fig. 2.

Assuming statistical independence of the temperatures (distributions) associated with each velocity component, the true axial temperature, T_A, can be calculated given the "temperatures" in the radial, T_R, and off axis, T_O, directions. This assumption yields an elliptical relationship:

$$\cos^2\left(\pi/2 - \alpha\right) + \left(\frac{T_R}{T_A}\right)^2 \sin^2\left(\pi/2 - \alpha\right) = \left(\frac{T_R}{T_O}\right)^2$$

Solving for the axial temperature yields

$$T_A = T_R \left[\frac{\left({}^{T_R}\!/\!_{T_O} \right)^2 - 1}{\cos^2(\alpha)} + 1 \right]^{-1/2}. \qquad (3)$$

Fluorescence Lineshape Model

Estimating the temperature required a model of the fluorescence spectral lineshape. A first-order approximation to modeling the lineshape of the

LIF signal was used for this study; a more detailed model of the hyperfine and isotopic line structure is under development.

Some broadening mechanisms such as natural lifetime, collisions, and transit time were neglected because of the low density and the small resonance time of the excited state. The model considered only Doppler broadening which assumes a Maxwell-Boltzmann distribution. Averaging over the Doppler shift of each velocity component in the distribution yields a Gaussian lineshape,

$$g(\nu) = \frac{c}{\nu_0}\left(\frac{m}{2\pi kT}\right)^{1/2} \exp\left[-4ln(2)\frac{(\nu - \nu_0)^2}{\Delta\nu_D^2}\right]$$

where $\Delta\nu_D$ is the full width at half maximum height (FWHM):

$$\Delta\nu_D = \frac{2\nu_0}{c}\left(\frac{2ln(2)kT}{m}\right)^{1/2}. \qquad (4)$$

Xe II LIF data from the low-temperature reference cell were fit with six arbitrarily-located Gaussians. The line centers and relative line strengths of the Gaussians were maintained in all subsequent reduction of Xe II LIF data. This provided a fair approximation of the temperature, as well as a diagnostic for any possible power broadening.

Similarly, data for Xe I LIF from the reference cell were also fit with six Gaussians. This fit appeared to agree well with data from different runs and was used to reduce all of the Xe I LIF data.

Centerlines and relative magnitudes for both Xe I and Xe II models are given in Table 1. The center of the primary Gaussian in the reference cell fit was taken as a zero velocity datum. Speeds were determined by the shift in this line incorporated in the entire fit.

Apparatus and Procedure

Cathodes

Two hollow cathode assemblies (HCAs) were used in this investigation. Both were provided to the University of Michigan by NASA GRC. Under an agreement with GRC the dimensions of the cathode orifices and details of their chamfering are not provided here.

One HCA was a prototype space station contactor with a 0.635 cm diameter hollow cathode. The keeper to cathode gap was 0.2 cm. A cylindrical anode approximated the conditions around the discharge cathode of an ion engine. The 6.35 cm anode diameter was chosen to facilitate comparison of data with previous investigations of ion velocities.[3,4] Four 7 cm axial slits cut into the anode facilitated observation of cathode operation, alignment of probes, and LIF measurements. Tests were performed with and without voltage applied to the anode electrode.

The other HCA was the "AR3" cathode used in HCA performance evaluation testing.[10] It incorporated a 0.318 cm diameter hollow cathode and a keeper plate located 0.4 cm downstream of the cathode orifice. The open keeper configuration permitted LIF in the cathode-to-keeper gap. The gap was increased from the nominal 0.2 cm to 0.4 cm because the keeper electrode extended several millimeters above the cathode and would have blocked the "axial" beam if it had not been retracted. This increase allowed interrogation at several data points. The physical phenomena existing in the gap was expected to be similar regardless of the gap length.

HCA handling and conditioning followed procedures derived from experience with the Space Station Plasma Contactor program.[10,11,12] These procedures ensured the best possible means to achieve similar cathode lifetimes, providing continuity to the research effort.

The HCAs were operated over a wide range of discharge currents and voltages. The principal limitations on the output power were the flow meter's maximum flow rate (5 sccm) and the anode wiring (8 A). Table 2 summarizes the operating conditions. The current/voltage settings of the HCAs were chosen to correspond to potential applications. However, the high operatiing current of a HCA in a space station contactor configuration was beyond the capability of the testing facility. In general, the operating conditions of the HCA with an anode were randomly chosen to present a mix of spot and plume modes over the range of testing capability.

Facility

These experiments were conducted in the Cathode Test Facility (CTF) at the Plasmadynamics and

Electric Propulsion Laboratory at the University of Michigan. The CTF has an inside diameter of 60 cm and a length of 245 cm. A 41 cm diameter cryogenic vacuum pump maintained a high vacuum in the chamber during testing, with a base pressure of approximately $7 \bullet 10^{-6}$ Pa; a cold cathode gage measured the pressure. The pump speed on Xe was approximately 1500 L/s. The CTF propellant feed system was designed and maintained as closely as possible to the specifications established in the contactor program.

In all measurements, the laser beams and the Langmuir probe were fixed and the HCA was moved to permit interrogation of points in the HCA plume. Three degrees of freedom were provided by two 30 cm translation stages (for axial and radial motion) and a lab jack with stepper motor (for vertical motion). The jack was mounted to a plate bolted to rails on the wall of the CTF; the axial stage was mounted on the jack, and the radial stage was mounted on the axial stage.

The two translation stages were controlled and monitored via a computer. Resolution was on the order of 0.025 cm for both stages. The jack was controlled manually, with a HeNe laser facilitating alignment. Resolution on the slow-moving jack was about 0.05 cm, corresponding to the laser spot size.

Laser and Optics

An argon-ion pumped Coherent dye laser (899-29 model) was used with Rhodamine-6G dye. Typical power was 0.25 W at 605 nm and 0.35 W at 582 nm. The laser wavelength was varied over 0.024 nm (20 GHz) in 0.061 pm (50 MHz) increments. This scanning and the synchronized data collection were computer controlled.

Because of the large natural fluorescence at both 529 and 618 nm, the laser beams are chopped in order to phase-lock the laser induced fluorescence. In order to distinguish velocity components, the "axial" beam was chopped at 1000 Hz while the radial beam was chopped at 880 Hz. About 10 percent of the radial beam was split off downstream of the chopper and passed through the center of a hollow cathode in a Hamamatsu opto-galvanic cell with Xe and Ne gases. The voltage applied across the opto-galvanic cell determines the plasma density and temperature: A dell voltage of 150 V produced an optimal LIF signature for Xe I, while 330 V gave a strong Xe II signal. A Chromex 0.5 m monochromator with a Hamamatsu 928 photo-multiplier tube (PMT) collected the fluorescence.

The laser and optics shown schematically in Fig. 1 are located in a controlled atmosphere/low-dust enclosure. The beams are delivered to the CTF and then to the cathode as shown in Fig. 3. The fluorescence from the cathode plume is collected by a small H1011 Spex monochromator with a Hamamatsu 928 PMT.

Operational amplifier circuits converted the PMT current signals to voltage signals. Lock-in amplifiers then isolated the fluorescence components of these signals, separating the CTF "axial" from the radial component. The Coherent 899-29 Autoscan software collected and matched the laser frequency to these signals. A Burleigh wave meter on loan from NASA GRC was used to verify the frequency of the laser.

Laser alignment was accomplished in two stages. A 0.0125 cm diameter Tungsten wire cross hair was placed 6 cm downstream of the keeper to facilitate rough alignment. The focal volumes of the two laser beams were overlaid on the cross hair, which was within 0.1 cm of the cathode orifice centerline. Fine alignment consisted of minimizing the radial Doppler shift (zero radial shift being centerline) and maximizing the signal strength of the "axial" Doppler shift.

Langmuir probe

A flat Langmuir probe with a 0.0125 cm diameter tip was used to measure plasma properties, especially plasma potential. Because severe erosion of a guard ring on the probe was observed in previous experiments, no conductor was placed on the external surface of the 0.075 cm diameter alumina insulator on the probe electrode.

Langmuir probes are subject to four "sheath" effects: deviation from quasi-neutrality, plasma density perturbation, ion energy depletion, and electron energy perturbation.[13] The significance of these effects depends on the mean-free-path, λ_m, of the plasma, which is estimated from Langmuir probe data. Previous measurements with a similar probe show that the mean free path of the plasma varies from 4.0 cm to roughly 40 cm. The sheath thickness will be on the order of $5 \bullet 10^{-2}$ cm. Since the probe diameter and sheath thickness are much

less than the mean free path, these sheath effects can be neglected.

The tip of the Langmuir probe was fixed 3.5 cm off axis from the interrogation point of the lasers. The cathode was moved back and forth, permitting interrogation by either the laser or the probe at the same point along the cathode axis. The probe was oriented normal to the axis of the cathode.
Alignment with the cathode centerline consisted of maximizing the measured electron number density, which was calculated in real time by the data acquisition software.

Results

Because the LIF signal strength was optimized at most points of interrogation, the data is presented in a self-normalized format. Periodically, a polarizer was used to vary the power of the laser beam upstream of the first beam splitter as a check for saturation and power broadening. No saturation or power broadening was observed.

1/4" Contactor HCA Ion Data

Figure 4 shows fluorescence data collected during an LIF interrogation 5 mm downstream of the keeper of the Contactor HCA operating in a 6 A spot-mode. The trends in Fig. 4 were typical of data taken at all locations and operating conditions of the Contactor. The slight offset of the radial signal indicates that the point of interrogation was slightly above the centerline of the cathode orifice. The effects of this were taken into account in reducing the axial component of the velocity via Eqn. 2. The relatively well-defined peaks facilitated the calculation of bulk speeds. However, uncertainty in the angle α between the two laser beams yielded a ten percent uncertainty in axial speeds.

Figure 5 gives the centerline axial velocity components for the four Contactor operating conditions. Note that there was a significant rise in the velocity of the ions a few centimeters downstream of the keeper face in all cases. No variation in axial speed $\pm$.0.5 and 1.0 mm off centerline was observed. This symmetry existed in both plume and spot modes.

The radial velocity was roughly 500 m/s in all spot-mode cases and varied from 600 to 950 m/s in plume mode. The trend of small, roughly constant radial velocities suggests that there was a slight alignment error since the radial velocity should be identically zero on centerline. If the HCA was at an angle, the radial velocity should vary with axial position. This slight misalignment introduced a negligible error in axial speed measurement.

While the magnitudes of each distribution are normalized, the line widths reflect the actual spreads in the data. Note that much of the structure observed in the reference cell signal is not present in the HCA data. Significantly reducing laser power in each beam did not reduce the line widths and did not reveal more structure. Reducing the lock-in time constants and increasing the time of the laser scan also had no effect.

The temperatures associated with each of the three signals were calculated by the model described above. The fits are shown in Fig. 4 as dashed lines. Failure of the model to fit more closely in the wings may result from the non-physical nature of the model, a non-Maxwellian distribution of ion velocities, noise amplified in the normalization, or some combination of these.

Figure 6 gives the temperature associated with the axial and radial measurements. The error bars reflect a ten percent uncertainty in fitting the data by hand. The values for spot-mode operation are roughly constant, varying between 0.5 and 1.5 eV. In plume-mode, the axial temperatures are larger and decrease significantly with axial position. The narrowing of the profiles most likely resulted from the migration of lower-energy ions from the centerline, leaving a narrower distribution of higher-energy ions.

1/8" AR3 HCA Ion Data

Figure 7 shows fluorescence data collected during an LIF interrogation 0.5 mm downstream of the keeper of the AR3 HCA operating in a 1.5 A plume mode. These data show typical trends for the AR3. The slight offset of the radial signal has been eliminated. As with the Contactor, the relatively well-defined peaks facilitated the bulk velocity calculations. Plume-mode LIF signal strengths were comparable to those of the Contactor; however, the spot-mode signals were much weaker.

Figure 8 gives centerline bulk axial speeds for the AR3 at various operating conditions. Ions moving towards the cathode orifice were consistently detected with energies of a few eV.

Figure 9 gives the temperatures associated with the axial and radial velocity distributions. Note that the axial velocity magnitudes were significantly higher than the radial.

Neutral Temperatures

Potentially, the temperature of the HCA plume can be approximated by the ion temperature. As an alternative, the temperature of neutral xenon, Xe I, was measured using LIF.

Figure 10 shows a typical Xe I LIF scan of the AR3 in plume-mode. Note the virtual overlap of the radial, axial, and reference profiles, implying that the bulk velocity of the neutrals was very small. The neutral signal was very strong in plume mode and very weak in spot mode.

Table 3 gives neutral temperatures at the exit plane of the AR3 cathode. These temperatures were nearly an order of magnitude below the radial ion temperatures. The temperatures dropped by fifty percent a few millimeters downstream of the cathode orifice.

Langmuir probe

Langmuir probe data were taken during operation of the AR3 HCA. The Langmuir probe measured floating potential, plasma potential, electron temperature, electron saturation current, and electron number density; these data were reduced graphically.

Data were taken during similar previous Contactor HCA operation. Quantitative comparisons between that investigation and the present one may not be accurate. Contactor HCA data are presented for qualitative comparison only.

Of particular interest to this investigation is the plasma potential, which should directly reveal the presence of a "potential hill." Figure 11 gives the plasma potential for several of the AR3 operating conditions and a couple Contactor operating conditions. The potentials varied, but there is no indication of a pronounced peak.

Discussion

The physical mechanism leading to ions traveling away from the negative electrode with energies greater than the discharge voltage is unclear. One theory posits the existence of a potential-hill downstream of the cathode.[14] In the region of this hill, electrons emitted by the cathode ionize the neutrals. The secondary electrons created by this ionization are able to escape but the heavier ions accumulate, inducing the potential-hill. Once the hill has started to develop, the potential continues to grow, establishing a state between ion ejection and trapped secondary electrons.[14]

The velocities at which ions escape from the hill away from the cathode are determined by the Bohm condition for a stable sheath.[14] Assuming both primary and secondary electrons, the Bohm velocity is

$$u_B = \left(\frac{kT_e}{m_i} \frac{n_{em} + n_{ep}}{n_{em} + \frac{kT_e}{2eV_p} n_{ep}} \right)^{1/2}, \qquad (5)$$

where

$$n_{em} = n_e \frac{z_0^2}{z^2} exp\left[\frac{e(V_P - V_a)}{kT_e} \right]$$

and

$$n_{ep} = \frac{J_e}{e\Omega \left(2eV_P / m_e \right)^{1/2} z^2}.$$

Either the peak potential or the velocity must be measured. The peak voltage, predicted to increase with electron temperature and to decrease with flow, is expected to be in the tens of eV for cathode operation. The current flowing back to the cathode has been found to be small.[14]

Table 4 gives potential peaks necessary to achieve some of the measured ion velocities. These values assume all of the ions were created at the peak of the hill. They are, therefore, lower limits on the peak potentials.

An alternate explanation of the high-energy ion production postulates an MPD effect.[15] In this model, the high-energy ions are accelerated by a

self-induced magnetic field in much the same way ions are accelerated in an MPD thruster. Considering the electrode diameters to be those of the cathode and keeper orifices, the electric field would have a significant radial component. A self-induced azimuthal magnetic field would result from the ion motion. This effect would be characterized by an almost instantaneous acceleration (jump) to a high velocity. The acceleration is provided both by the crossing of the radial arc current with the self-generated magnetic field and by axial components of the arc current crossing with the azimuthal magnetic field, yielding a radial gradient in the gasdynamic pressure.[16] These two effects can be integrated over the cathode face, yielding

$$F = \frac{\mu J^2}{4\pi}\left[ln\left(\frac{r_a}{r_c}\right) + \frac{3}{4}\right]. \qquad (6)$$

For a flow rate on the order of 1 sccm and a current of 6 A, the exit velocity would be on the order of 0.075 m/s. Indeed, an upper bound to the exhaust speed derived from the magnetic field is

$$u \le \frac{\mu e J}{2\pi m_i}. \qquad (7)$$

For 6 A, this yields a limit of roughly 5 m/s. Thus, even though the data may qualitatively suggest this mechanism, it seems to have negligible impact.

1/4" Contactor HCA

The Contactor data was consistent with a potential-hill located downstream of the keeper. In most cases, it would have to be within the first 2 mm. However, the 6 A plume-mode case indicates the presence of a hill roughly 10 mm from the keeper.

The observation of higher-energy ions in both spot-mode and plume-mode is consistent with several previous investigations.[1,2,6,17] As expected, the peak energy is higher for the ions generated in plume mode (higher electron temperature and lower flow rate for the same current). The relative axial peak locations are also consistent with previous Langmuir probe measurements.[18]

The low velocities near the keeper may indicate a pre-acceleration region very near the keeper orifice. This phenomenon may result from the very high density of ions near the orifice in spot-mode.

The temperatures are lower than those observed using different techniques.[1,5] In general, this investigation would tend to lend itself to over-predicting rather than under-predicting the width. Saturation, power-broadening, poor spatial resolution, and time-constant smoothing would all tend to broaden the width. While these were actively avoided via periodic variations in laser operating conditions, their absence would not tend to artificially narrow the spectrum.

1/8" AR3 HCA

With the exception of the 0.5 A operating condition, there was no evidence of a potential hill in the cathode-keeper gap. The small speeds measured at the cathode exit plane in the 0.5 A case may result from a slight misalignment.

The absence of a peak in the spot mode data may result from low-power operation. In plume-mode, failure to detect a hill might result from a peak downstream of the keeper. The extended gap might also affect the high-energy ion production.

Neutral temperatures

To lend physical foundation to the LIF-measured neutral particle temperatures, a theoretical model was developed to predict the heavy particle temperatures in the hollow cathode. Salhi[22] first derived this model for the radial distribution of heavy particle temperatures from a discussion of equipartition in a two-temperature plasma in Spitzer.[23] The neutrals are assumed to equilibrate with the ions over length scales much shorter than the dimensions of the cathode. Consequently the heavy particle temperature distribution is modeled by solving the one-dimensional, time-dependent heat transfer equation

$$\frac{1}{r}\frac{d}{dr} r\kappa \frac{dT_h}{dr} = \rho c_p \frac{dT_h}{dt}. \qquad (8)$$

The time derivative is defined according to Spitzer:[23]

$$\frac{dT}{dt} = \frac{T_i - T_e}{t_{eq}},$$

where t_{eq} is the equipartion time. Spitzer[23] reports the convenient form of the equipartion time as:

$$t_{eq} = 5.87 \frac{M_e M_i}{n_e Z_e^2 Z_i^2 \ln\Lambda}\left(\frac{T_e}{M_e} + \frac{T_i}{M_i}\right)^{3/2}. \qquad (9)$$

The thermal conductivity was calculated using the mean free path method,[22,24]

$$\kappa = \frac{2k}{\sigma}\sqrt{\frac{kT_h}{\pi m_h}},$$

and the density and specific heat were rewritten using the kinetic description[25]

$$\rho c_p = n_e m_h \left(\frac{3}{2}\frac{k}{m_h}\right) = \frac{3}{2} n_e k. \quad (10)$$

The model by Mandell and Katz[25] was used to obtain estimates of the electron temperature and number density within the orifice. The predicted number densities varied from 5 x 10^{14} to 1 x 10^{16} cm^{-3}, and the number densities ranged between 1.8 and 2.3 eV. The boundary conditions for the differential equation were zero radial temperature gradient on axis and heavy particle temperature equal to the wall temperature at $r=r_o$.

When solving for the radial heavy particle temperature profile, sharp gradients were obtained near the wall at number densities well below those predicted using the model in.[25] As shown in Fig. 12, the heavy particle temperature equilibrates with the electron temperature away from the wall of the orifice. The conditions used to generate Fig. 12 are significantly less favorable for equilibrium than those predicted using the orifice model or even those measured in the insert region.[22] The temperature gradient near the wall made the solution of the differential equation unstable at the electron temperatures and number densities expected in the orifice region. As a check of the hypothesis that the bulk of the heavy particles are in equilibrium with the electrons, the relation

$$\frac{T_e - T_i}{T_e} = \frac{M_i}{8M_e}\frac{\left(\lambda_e eE\right)^2}{\left(\tfrac{3}{2}kT_e\right)^2}, \quad (11)$$

which determines the deviation between electron and ion temperatures, was evaluated using an estimate of the field strength in the orifice, and the results showed approximate equality between electron and ion temperatures for the conditions in the orifice of the hollow cathode.[22] Consequently, the experimentally determined ion and neutral temperatures reported here were physically justified. The authors point out that this prediction may not be valid for plume mode characteristics due to the large transients in the plasma which are not taken into account in this derivation. However, this model predicts the experimentally observed trend that the heavy particle temperatures increase in plume mode due to the elevated electron temperatures.[9]

Langmuir probe

The plasma potentials measured in the cathode-keeper gap agree with the LIF data. No potential peaks were detected with either diagnostic.

It is possible that the failure to detect a potential hill both in and beyond this gap resulted from misalignment of the probe with the center of the cathode orifice. However the relatively large region in which this peak should be detected (across the 2 mm cross-section of constant velocity) would tend to mitigate against this.

Conclusions

Laser induced fluorescence was demonstrated to be a viable technique for interrogating the ion plumes of hollow cathode assemblies. The multiplex technique permitted repeatable, reliable measurement of ion speeds up to several centimeters downstream of the HCA.

The LIF data tends to support the "potential-hill" theory of high-energy ion production in HCA operation. This is especially true for plume-mode operation, even though no peaks were detected with the Langmuir probe. The relatively small temperatures may result from the first-order model used to reduce them. However, they may also indicate that the broader distributions observed in other investigations result from doubly or singly charged ions, collisional broadening, or integration of off-axis ions. This would be consistent with (but not necessarily supported by) other investigations which illustrate these effects.[19,20,21] A more accurate model of the ion energy distribution has been developed.[21]

The difference in Xe I and Xe II temperatures may indicate that the ion velocity distribution was not an accurate indication of the ion temperature and/or that Xe I and Xe II were not in thermodynamic equilibrium. The observed temperatures, when used in an equation of state, were consistent with the

internal cathode pressures observed during operation.

Finally, the observation of ions being accelerated back towards the cathode orifice indicate that this LIF technique will be of value in mapping the ion velocity profiles near the exit of the discharge cathode of an ion engine. That investigation will take place in the near future.

Acknowledgments.

This work was made possible by the continuing support of NASA GRC and the personnel associated with the On-Board Propulsion Branch. Of special support has been M. Patterson. The research has been carried out under NASA Grants NAG 31572 and NAG-32216 monitored by J. Sovey.

Significant advice and support from D. Keefer and N. Wright at UTSI and from L. Erman of Coherent Lasers are gratefully acknowledged. The authors would also like to thank the Department's technicians and the other students in the PEPL group for their assistance and support.

References

1. Kameyama, I., and P. J. Wilbur, "Characteristics of Ions Emitted from High-Current Hollow Cathodes," IEPC-93-023, 23rd International Electric Propulsion Conference, (August, 1993).

2. Kameyama, I., and P. J. Wilbur, "Effects of External Flow Near High-Current Hollow Cathodes on Ion-Energy Distributions," IEPC-97-173, 25th International Electric Propulsion Conference, (August, 1997).

3. Patterson, M. J., et al, "2.3 kW Ion Thruster Wear Test," AIAA-95-2516, 31st Joint Propulsion Conference, (July, 1995).

4. Polk, J. E., et al, "A 1000 Hour Wear Test of the NASA NSTAR Ion Thruster," AIAA-96-2784, 32nd Joint Propulsion Conference, (July, 1996).

5. Friedly, V. J., and P. J. Wilbur, "High Current Hollow Cathode Phenomena," *Journal of Propulsion and Power*, Vol. 8, No. 3, 1992 635-643.

6. Manzella, D. H., "Stationary Plasma Thruster Ion Velocity Distribution," AIAA-94-3141, 30th Joint Propulsion Conference (June, 1994).

7. Cedolin, R. J., et al, "Laser-Induced Fluorescence Diagnostics for Xenon Hall Thrusters," AIAA-96-2986, 32nd Joint Propulsion Conference (July, 1996).

8. Gaeta, C. J., et al, "Erosion Rate Diagnostics in Ion Thrusters Using Laser Induced Fluorescence," *Journal of Propulsion and Power*, Vol. 9, No. 3, 1993, 369-376.

9. Domonkos, M. T., Gallimore, A. D., Williams, G. J., and Patterson, M. J., "Low-Current Hollow Cathode Evaluation," 35th AIAA / ASME / SAE / ASEE Joint Propulsion Conference, Los Angeles, CA, June 1999.

10. Keefer, D., et al, "Multiplexed Laser Induced Fluorescence and Non-Equilibrium Processes in Arcjets," AIAA-94-2656, 25the Plasmadynamics and Lasers Conference, (July, 1992).

11. Patterson, M. J., Verhey, T. R., Soulas, G., and Zakany, J., "Space Station Cathode Design, Performance, and Operating Specifications," IEPC Paper No. 97-170, *25th International Electric Propulsion Conference*, Cleveland, OH, Aug. 1997.

12. Sarver-Verhey, T. R., "Extended Test of a Xenon Hollow Cathode for a Space Plasma Contactor," NASA Contractor Report 195402, Nov. 1994.

13. Schott, L., "Electrical Probes," *Plasma Diagnostics*, W. Lochte-Holgreven ed., AIP Press, Woodbury, NY, 1995 pp 668-725.

14. Kameyama, I., and P. J. Wilbur, "Potential-Hill Model of High-Energy Ion Production Near High-Current Hollow Cathodes," ISTS-98-Aa-2-17, 21st International Symposium on Space Technology and Science, (May, 1998).

15. Brophy, J. R., and C. E. Garner, "Tests of High Current Hollow Cathodes for ion

Engines," AIAA-88-2913, 24th Joint propulsion Conference, (July, 1988).

16. Jahn, R. G., *Physics of Electric Propulsion*, McGraw Hill, New York, 1968, pp 240-248.

17. Williams, J. D., and P. J. Wilbur, "Electron Emission from a Hollow Cathode-Based Plasma Contactor," *Journal of Spacecraft and Rockets*, Vol. 29, No. 6, 1992, 820-829.

18. Siegfried, D. E., and P. J. Wilbur, "An Investigation of Mercury Hollow Cathode Phenomena," AIAA-78-705, 13th International Electric Propulsion conference, (April, 1978).

19. King, L. B., and A. D. Gallimore, "Ion Energy Diagnostics in the Plume of an SPT-100 from Thrust Axis to Back Flow," AIAA-98-3641, *34th Joint Propulsion Conference*, Cleveland, OH July, 1998.

20. Gulczinski, F. S., R. R. Hofer, and A. D. Gallimore, "Near-Field Ion Energy and Species Measurement of a 5 kW Laboratory Hall Thruster," AIAA-99-2430, 35the Joint Propulsion Conference (June, 1999).

21. Williams, G. J., et al, "Laser Induced Fluorescence Measurement of the Ion Energy Distribution in the Plume of a Hall Thruster," AIAA-99-2424, 35th Joint Propulsion Conference, (June, 1999).

22. Salhi, A., "Theoretical and Experimental Studies of Orificed, Hollow Cathode Operation," Ph.D. Dissertation, Ohio State University, 1993.

23. Spitzer, L., *Physics of Fully Ionized Gases*, John Wiley & Sons Interscience Publishers, New York, 1962.

24. Gombosi, T. I., *Gaskinetic Theory*, Cambridge University Press, Great Britain, 1994.

25. Mandell, M. J. and Katz I., "Theory of Hollow Cathode Operation in Spot and Plume Modes," AIAA Paper No. 94-3134, 30th AIAA / ASME / SAE / ASEE Joint Propulsion Conference, Indianapolis, IN, June 1994.

26. Eckert, E. R. G. and Pfender, E., "Advances in Plasma Heat Transfer," in Advances in Heat Transfer, Vol. 4, Academic Press, New York, 1967

Table 1 Parameters for the first order lineshape model.

Fit	Xe I Centerline (nm)	Xe I Magnitude	Xe II Centerline (nm)	Xe II Magnitude
Gaussian 1	528.547023	0.94	605.282146	0.84
Gaussian 2	582.546061	0.55	605.283368	0.33
Gaussian 3	582.548201	0.355	605.279873	0.30
Gaussian 4	582.549548	0.05	605.280985	0.18
Gaussian 5	582.544759	0.05	605.284033	0.08
Gaussian 6	582.543933	0.035	605.285866	0.05

Table 2 HCA Operating conditions.

Designation	Keeper Current (A)	Keeper Voltage (V)	Anode Current (A)	Anode Voltage (V)	Mass Flow Rate (sccm)	Facility Pressure (10^{-5} Torr)
1/4" Contactor HCA						
4 A, spot-mode	4.03	13.07	-	-	2.3	1.5
4 A, plume-mode	4.03	11.61	-	-	4.0	3.1
6 A, spot-mode	2.15	10.24	4.00	16.90	4.0	2.9
6A, plume-mode	0.00	0.00	6.05	28.1	4.0	3.0
1/8" AR3 HCA						
0.5 A, plume-mode	0.50	21.5	-	-	1.0	0.7
1.0 A, spot-mode	1.00	16.99	-	-	3.0	2.1
1.0 A, plume-mode	1.05	24.3	-	-	1.0	0.7
1.5 A, spot-mode	1.50	15.2	-	-	3.0	3.1
1.5 A, plume-mode	1.49	25.9	-	-	1.0	0.8

Table 3 Neutral temperatures.

Cathode Condition	Axial Temperature (K)	Radial Temperature (K)	Downstream Position
:0.5 A, plume-mode	2000	1800	0.5 mm from cathode
1.5 A plume-mode	3500	4000	0.5 mm from cathode
6.0 A spot-mode	2250	-	0.5 mm from keeper
6.0 A plume-mode	5000	-	0.5 mm from keeper

Table 4 Potential-hill peak prediction.

Cathode/Condition	Necessary Peak (V)
Contactor: 4 A, spot-mode	27
Contactor: 4 A, plume-mode	45
Contactor: 6 A, spot-mode	30
Contactor: 6 A, plume-mode	50
AR3: 0.5 A plume-mode	50

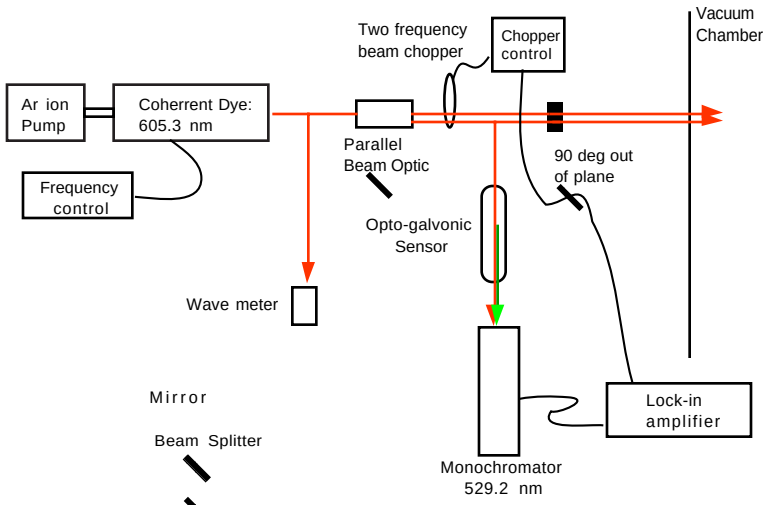

Fig. 1 Laser beam division and modulation.

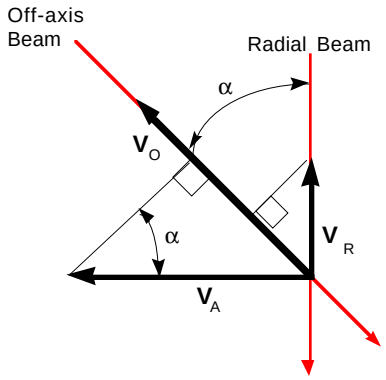

Fig. 2 Relationship between measured, V_0 and V_R, and calculated, V_A, velocities using the multiplex approach.

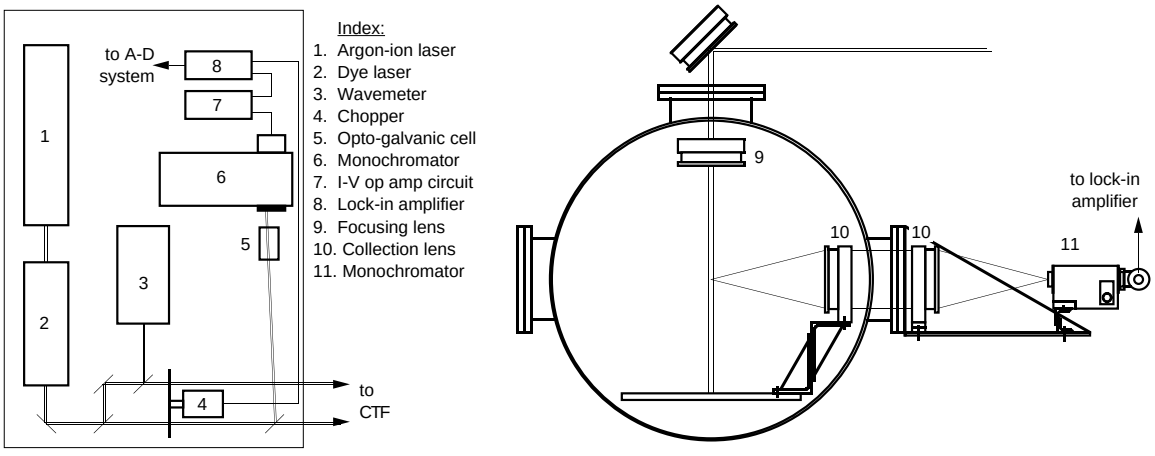

(a) Laser and reference cell setup (b) Cathode test facility (CTF) setup

Fig. 3 A schematic of the laser delivery and collection at the CTF.

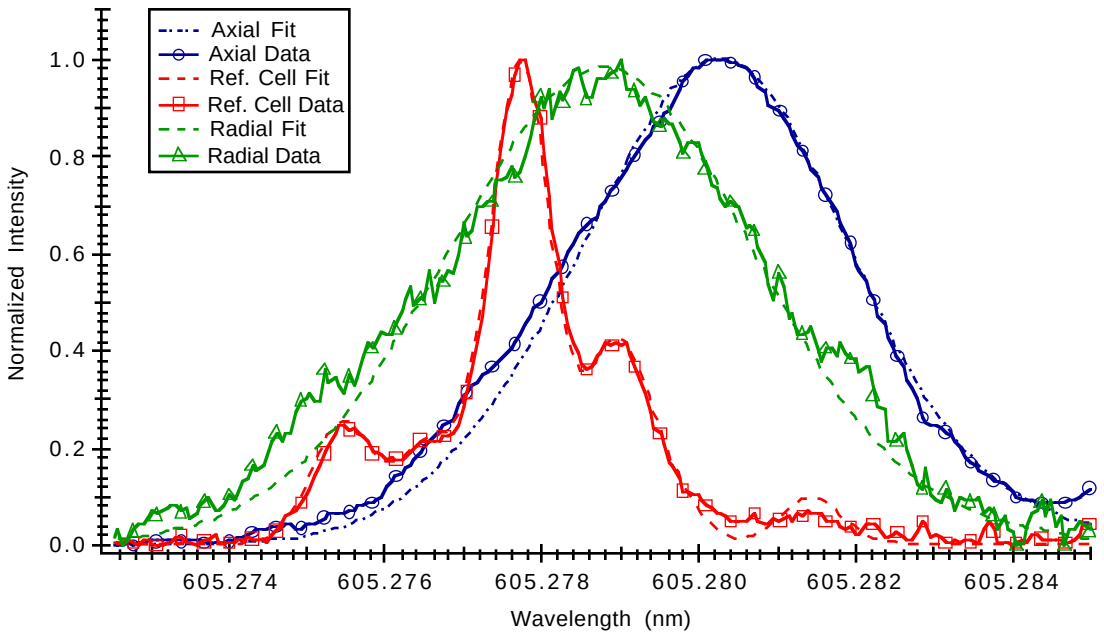

Fig. 4 Typical Xe II LIF scan data of the 1/4" Contactor HCA. Data shown were taken 5 mm downstream of the keeper in 6 A spot-mode operation.

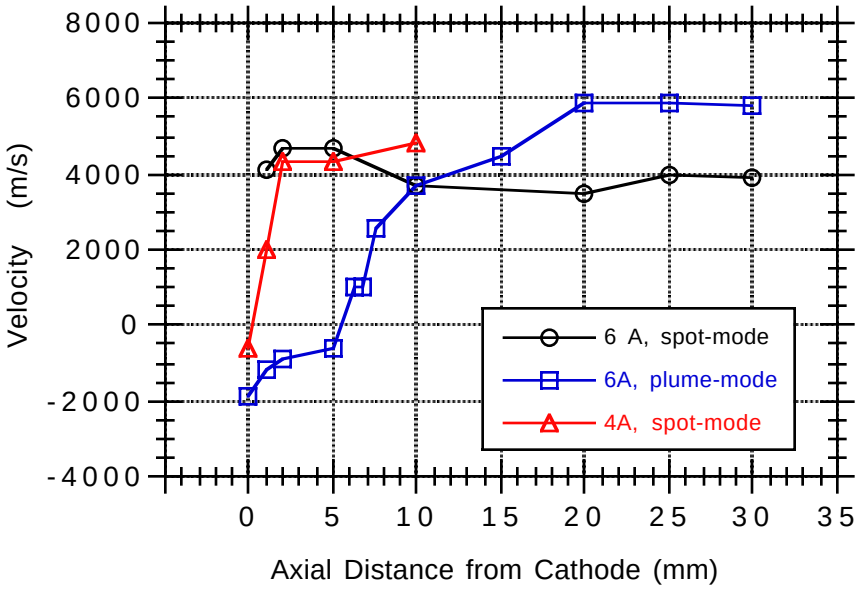

Fig. 5 Axial velocities for the Contactor HCA over various operating conditions.

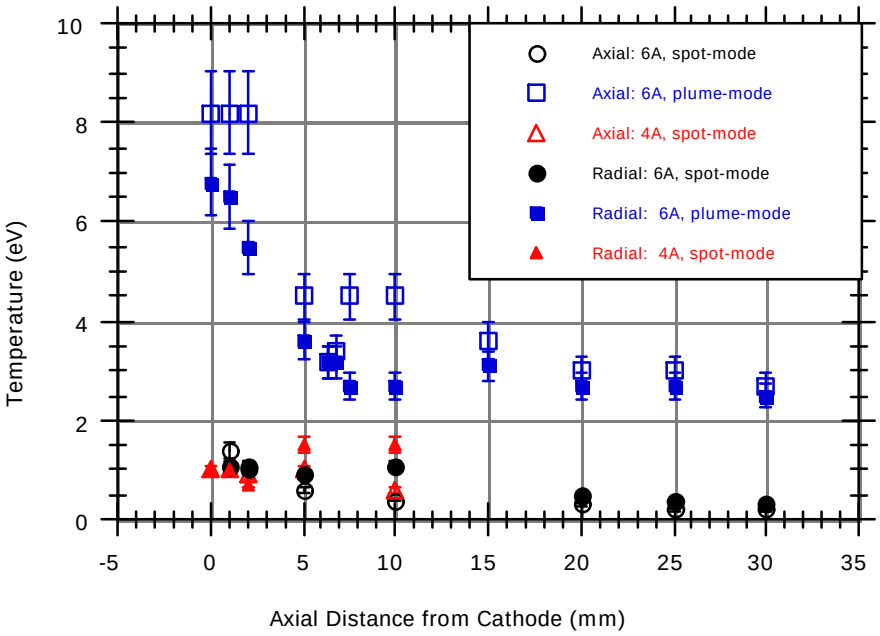

Fig. 6 Temperatures measured at different axial positions over various operating conditions of the Contactor HCA.

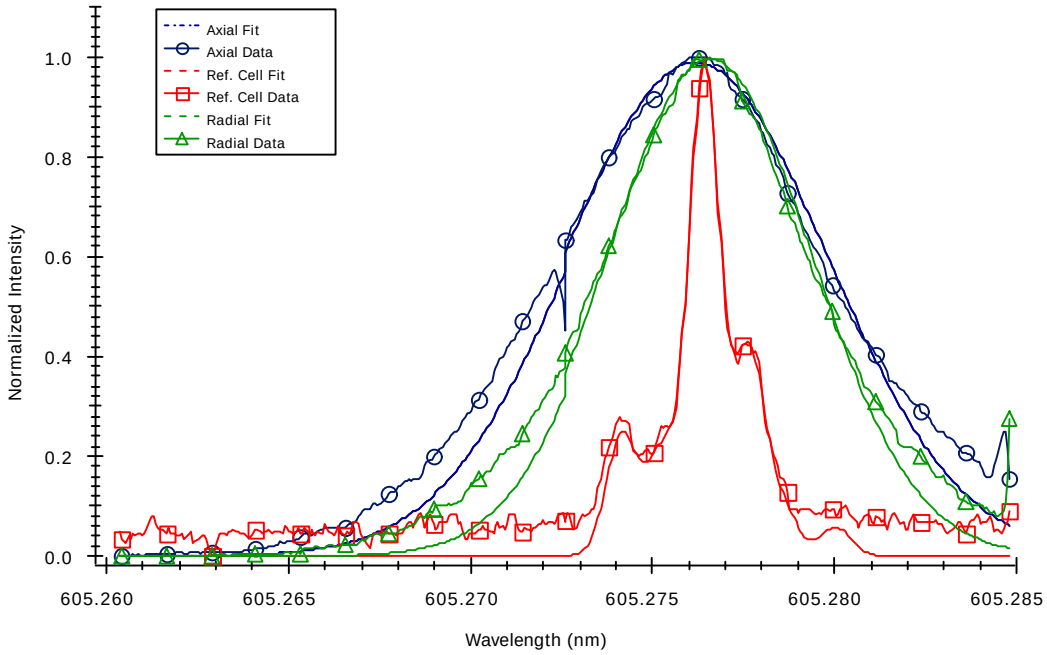

Fig. 7 Typical Xe II LIF scan data of the 1/8" AR3 HCA Data were taken 0.5 mm downstream of the cathode in 1.5 A, plume-mode operation.

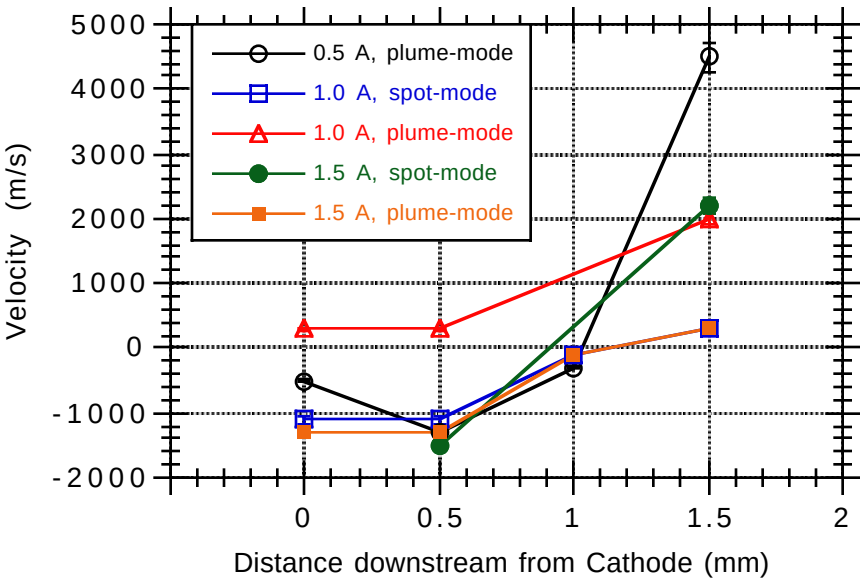

Fig. 8 Axial velocity distributions for the AR3 HCA over various operating conditions.

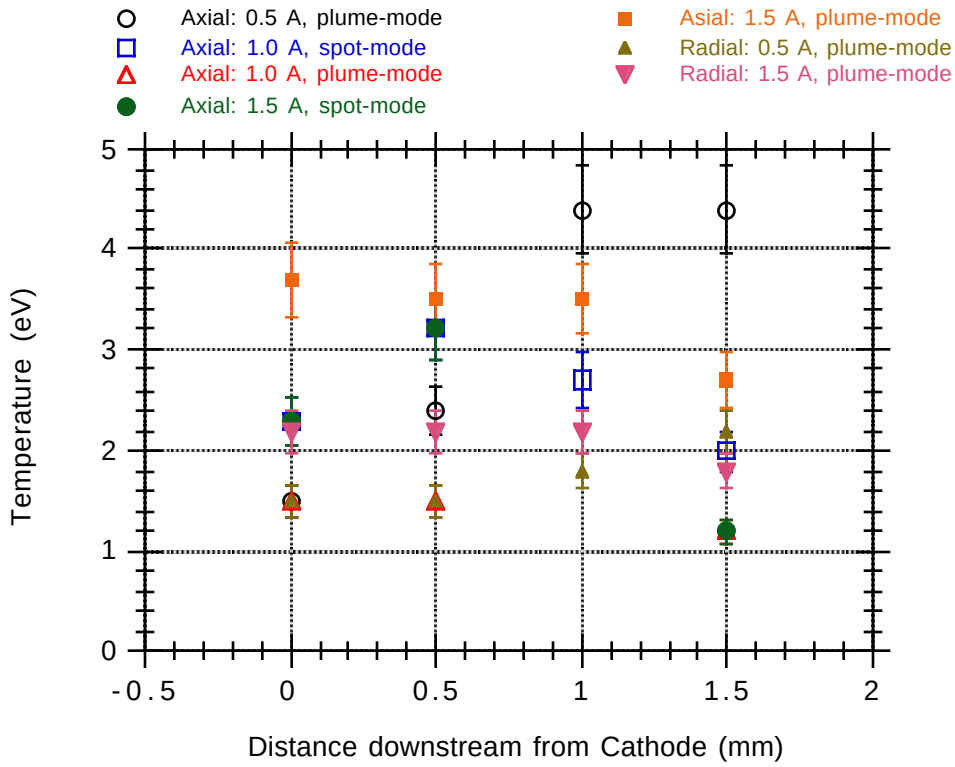

Fig. 9 Temperatures measured at different axial positions over various operating conditions of the AR3 HCA.

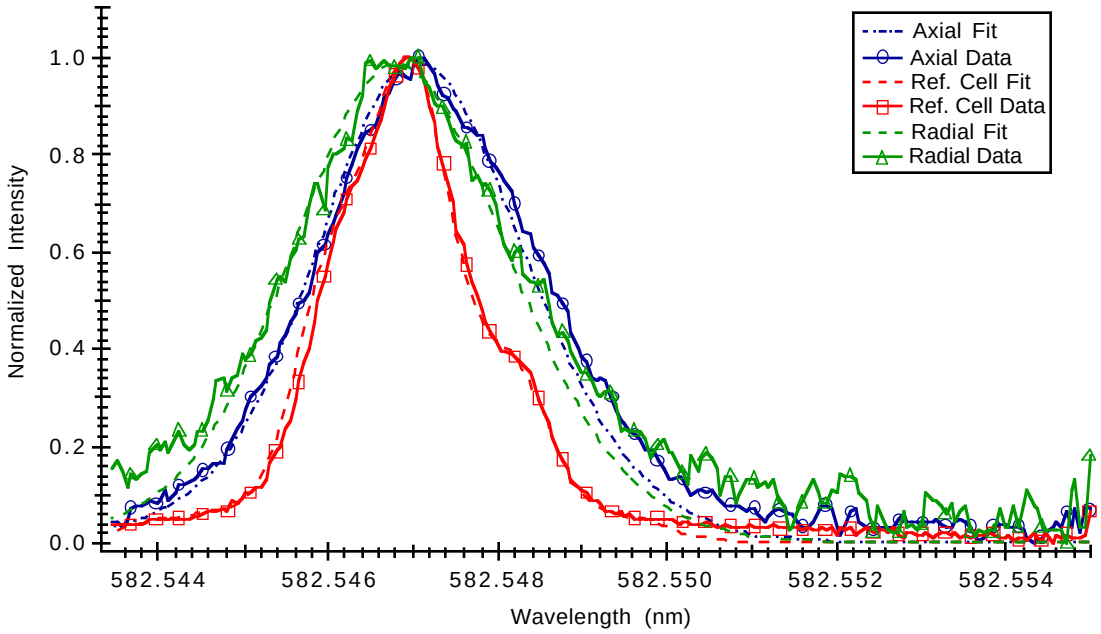

Fig. 10 Typical Xe I LIF scan data of the AR3 HCA. Data shown were taken 0.0 mm downstream in 1.5 A plume-mode operation. The data were similar for the Contactor.

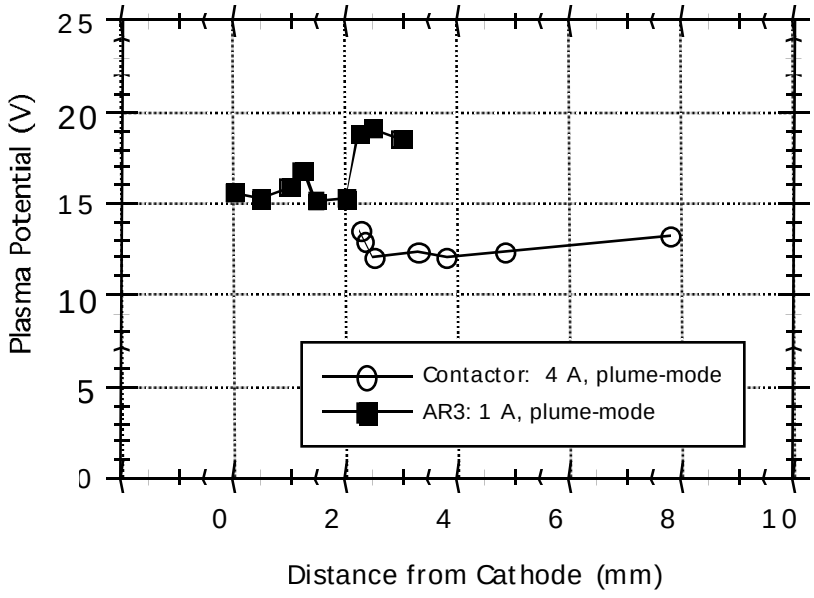

Fig. 11 Plasma potential downstream of the two HCA's for various operating conditions.